Atomic structure of interfaces between Mn3O4 precipitates and Ag studied with HRTEM

Kooi, B.J.; Groen, H.B; de Hosson, J.T.M.

Published in:
Acta Materialia

DOI:
10.1016/S1359-6454(97)00054-2

Publication date:
1997

Pergamon

Acta mater. Vol. 45, No. 9, pp. 3587–3607, 1997

Printed in Great Britain
PII: S1359-6454(97)00054-2
1359-6454/97 $17.00 + 0.00

ATOMIC STRUCTURE OF INTERFACES BETWEEN Mn_3O_4 PRECIPITATES AND Ag STUDIED WITH HRTEM

B. J. KOOI, H. B. GROEN and J. Th. M. DE HOSSON

Department of Applied Physics, Materials Science Centre, University of Groningen, Nijenborgh 4, 9747 AG Groningen, The Netherlands

(Received 28 October 1996; accepted 27 January 1997)

Abstract—Internal oxidation of Ag–3 at.% Mn resulted in Mn_3O_4 precipitates with a "parallel" topotaxy with the metal matrix and an octahedron shape due to {111} facets. Orientation and shape of Mn_3O_4 in Ag are not in the lowest strain energy state, indicating the dominance of interfacial energy over strain energy. Owing to the tetragonality of Mn_3O_4, only a few planes and directions of Ag and Mn_3O_4 can be parallel simultaneously. The precipitates exhibited a tendency to align {111} planes parallel with the matrix for one pair of facets and then for another pair a tilt of 7.6° occurs which is relieved by ledges in Ag. The dislocation structure at these parallel and tilted {111} interfaces, including phenomena such as stand-off and dissociation of (partial) dislocations, is scrutinized combining HRTEM and atomistic calculations. © *1997 Acta Metallurgica Inc.*

1. INTRODUCTION

To a large extent the potentially excellent properties of metal–oxide composite materials are affected by the chemical composition and structure of the interfaces. Coupling understanding of the interface at the atomic scale (chemistry, interatomic bonding, structure, defects) and properties of the interface and composite at the macro-scale may be an important route for tailoring metal–ceramic composite materials. HRTEM (combined with local chemical analysis) is particularly suited for the investigation of the interface at an atomic scale. Internal oxidation is a simple method to obtain clean interfaces between oxide precipitates and metal matrix. Then, the metal–oxide system under study and the conditions during oxidation determine the orientation relationships (ORs) and the interface orientations (IOs) [1]. Internal oxidation of metals with several valence states (or which give polymorphic oxides) may result in the formation of oxide phases with various crystal structures and may involve phase transformations.

Within this framework manganese oxide precipitates in Ag and Cu as obtained by internal oxidation were studied by HRTEM. The present paper deals with Mn_3O_4 precipitates in Ag and another paper with MnO and Mn_3O_4 precipitates in Cu [2]. Mn_3O_4 has a tetragonal distorted spinel structure (*I4/amd*) and compared to the f.c.c. lattice of Ag a misfit not only in size but also in shape is present. The fashion in which oxide precipitate and metal matrix cope at an atomic scale with misfit in size and shape between their lattices is the central question addressed.

2. EXPERIMENTAL

An alloy of silver containing 3 at.% manganese was made in a high-frequency furnace by melting the pure constituents (purity 99.99% by weight) in an alumina crucible under oxygen-free argon protective atmosphere. The ingot was homogenized (1 week at 700°C in an evacuated quartz tube) and subsequently cold rolled from 4 mm down to 0.5 mm. Oxidation was performed in air at 900°C for 1 h.

TEM samples were prepared by grinding, dimpling and ion milling 3 mm discs to electron transparency. For HRTEM a JEOL 4000 EX/II, operating at 400 kV (spherical aberration coefficient: 0.97 ± 0.02 mm, defocus spread: 7.8 ± 1.4 nm, beam semi-convergence angle: 0.8 mrad) equipped with an on-axis Gatan PEELS was used. HRTEM negatives were digitized and the grey scale adapted to achieve reasonable contrast. No filtering of images was performed. HRTEM image simulation was performed with MacTempas (supported by CrystalKit) [3] and also by EMS [4] when relaxed atomic configurations of (the metal at) the interface as obtained by the program described in Ref. [5] was used as input.

3. RESULTS AND DISCUSSION

3.1. Precipitate formation

Internal oxidation of Ag–3 at.% Mn in air at 900°C (1 h) resulted according to SAED patterns and HRTEM images in Mn_3O_4 (tetragonal distorted spinel, *I4/amd* [6]) precipitates; see Fig. 1. Possibly, instead of Mn_3O_4 γ-Mn_2O_3, a deficit arrangement of Mn_3O_4 with almost identical lattice constants, is

present. The differences between simulated HRTEM images of γ-Mn_2O_3 and Mn_3O_4 are very small and do not allow discrimination between the two phases on the basis of experimental HRTEM images, in a similar way as was performed for γ-Al_2O_3, η-Al_2O_3 and η'-Al_2O_3 in Ref. [7]. The OR between the precipitates and the matrix found can be regarded as parallel topotaxy (i.e. cube-on-cube, if Mn_3O_4 is for

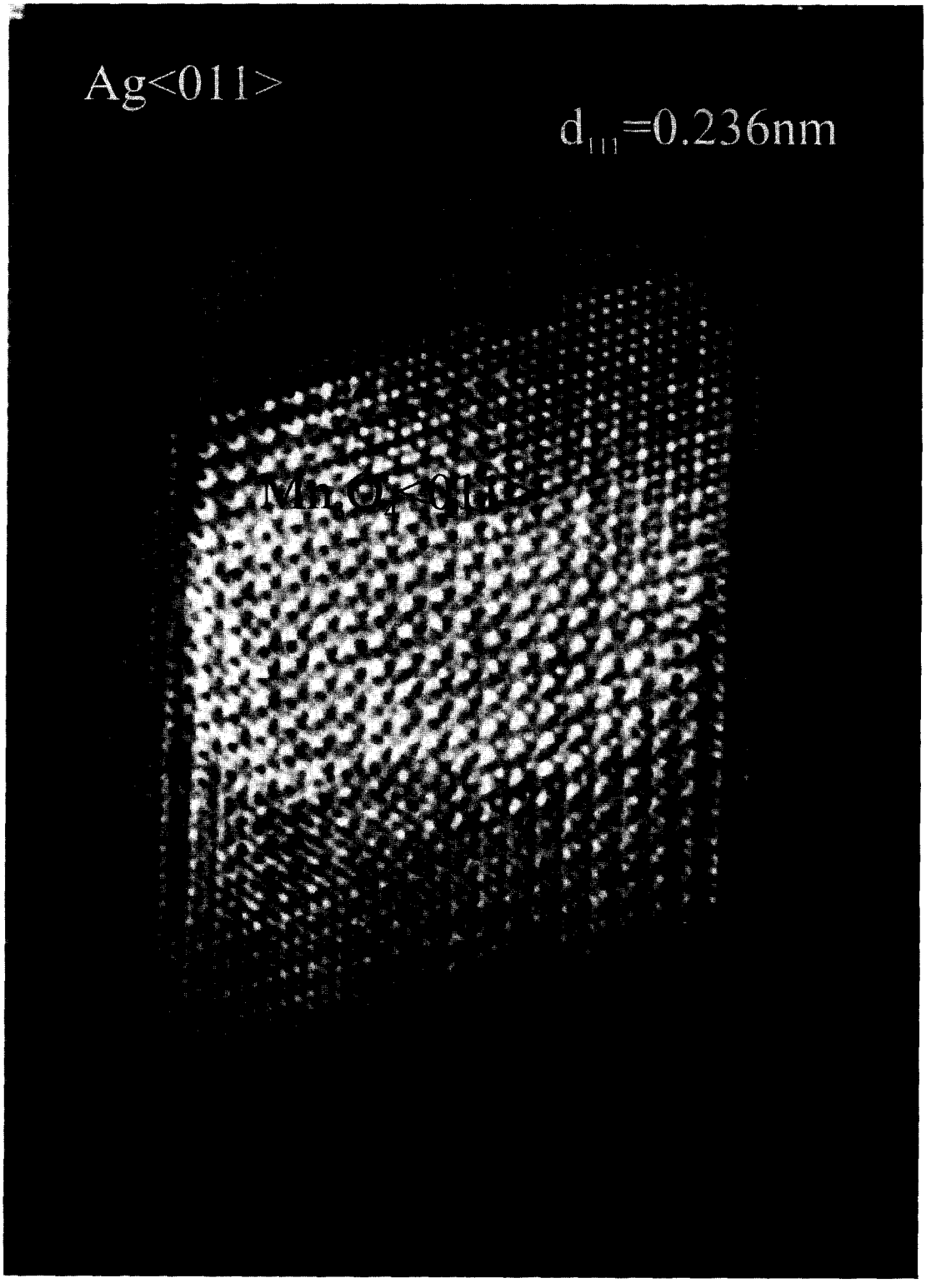

Fig. 1. *Caption on facing page.*

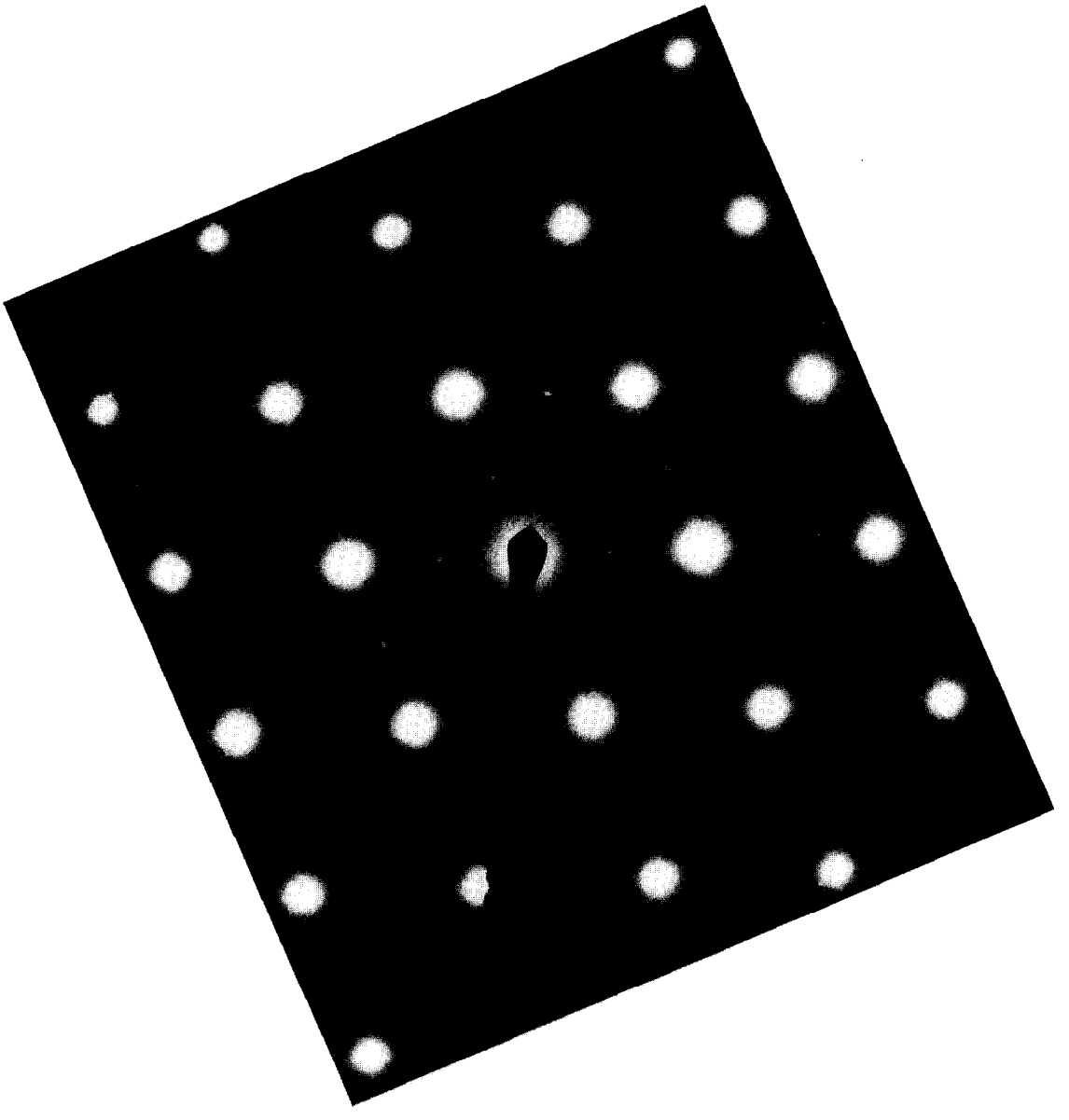

Fig. 1. HRTEM image of an Mn_3O_4 precipitate with $\{111\}$ facets in Ag; viewing direction along the $\langle 011 \rangle$ of Ag. (b) SAED pattern of superimposed $\langle 110 \rangle$ Mn_3O_4, $\langle 011 \rangle$ Mn_3O_4 and $\langle 110 \rangle$ Ag.

simplicity assumed to be cubic spinel), but due to the tetragonality of Mn_3O_4 parallelism is restricted to a few planes and directions at a time (which will be discussed extensively below). The precipitates have octahedron shapes owing to $\{111\}$ facets (usually no truncation due to $\{100\}$ facets is observable) and have a size of 5–20 nm. To allow maximum similarity with Ag, Laue indices of Mn_3O_4 in the following are based on tetragonal spinel and not on *I4/amd*, i.e. [100] and [010] for tetragonal spinel correspond to [110] and $[\bar{1}10]$ for *I4/amd*. Precipitates with (truncated) octahedron shape were earlier observed for oxides with NaCl structure in f.c.c. metals: MnO in Cu [8], MgO precipitates in Cu [9–12] and CdO in Ag [13]. As compared to these systems the tetragonal distortion of Mn_3O_4 in particular brings about interesting effects.

3.2. Mismatch in size and shape between Ag and Mn_3O_4

The mismatch between Mn_3O_4 and Ag is anisotropic; the a-axis of the tetragonal spinel is almost exactly twice the lattice constant of Ag (-0.4% mismatch) and the c-axis is 15.3% longer than twice the lattice constant of Ag. On the basis of mismatch, i.e. strain energy, the precipitate shape expected is a plate with (001) as dominant facet (see Table 1, where the strain energy on the basis of anisotropic linear elasticity is given for different parallel interfaces for Mn_3O_4 and hypothetical MnO

Table 1. Strain energy on Ag/MnO (hypothetical) and Ag/Mn_3O_4 interfaces for parallel interface orientation and different interfacial planes as calculated with anisotropic linear elasticity. Interfacial energy for parallel {111} Ag/MnO (hypothetical) and Ag/Mn_3O_4 interfaces is according to atomistic calculations. At the Ag/MnO interface an isotropic strain of 8.3% is present and at the Ag/Mn_3O_4 interface a strain of 10.0% is present only in the [11$\bar{2}$] direction; α denotes the factor allowing simulation of different interaction strengths across the interface (see text)

Ag//		MnO (GPa)	Mn_3O_4 (GPa)
Elasticity	{100}	1.67	1.4
	{001}	1.67	$4\ 10^{-3}$
	{111}	1.83	0.8
Atomistic		8.3%, $\alpha = 2$	10.0%, $\alpha = 2$
	{111}	-977 mJ/m^2	-1031 mJ/m^2 (undissociated 1/3 [11$\bar{2}$])
	{111}		-1188 mJ/m (dissociated 1/3 [11$\bar{2}$])

precipitates in Ag). However, this shape is not observed; it is an octahedron with {111} facets. Apparently, the interfacial energy between Ag and Mn_3O_4 dominates over the strain energy. The decrease in interfacial energy by changing the (001) facet into {111} facets outweighs the increase in strain energy. The difference in interfacial energy between the {001} and the {111} can be readily understood since at the {111} interface the terminating layer of the precipitate is most likely a close-packed oxygen layer, while at the {001} interface the less-densely and less-regularly packed terminating layer consists, for example, of both oxygen and manganese atoms in a ratio of 2:1. This result and interpretation is supported by recent *ab initio* calculations on adhesive energy and charge transfer for MgO/Cu heterointerfaces where two polar {111} (O and Mg terminated oxide) and two non-polar {100} (O and Cu and Mg over Cu) MgO/Cu interfaces have been considered [14]. The Cu in-plane lattice constant was stretched to match that of MgO giving a coherent interface. The polar interfaces were shown to exhibit significantly larger adhesive energies and charge transfer than the non-polar interfaces. It can be expected in general that interfacial energy dominates over strain energy at metal/oxide interfaces, whereas strain energy is expected to be more important for metal heterointerfaces than for metal/oxide interfaces.

However, it cannot be stated that the precipitate shape in Ag is always an octahedron with {111} facets without observable truncation due to {001} facets. An example of the exception is shown in Fig. 2; the precipitate shape is a truncated octahedron with a very large (001) facet, which size is about 1.5 (in other cases even more) times the size of a {111} facet. Only for 6 precipitates out of about 1000 which passed in review was this shape observed and in all 6 cases it turned out, as expected, to be an (001) facet [and not (100) or (010)].

Owing to the tetragonality of Mn_3O_4, parallelism of principal axes implies that the eight {111} facets of Mn_3O_4 are not parallel to the {111} planes of Ag; the normal of the {111} planes in Mn_3O_4 make an angle of 58.6° with the [001] axis, whereas for a cubic structure this angle is 54.7°. This misalignment can be easily observed in HRTEM images. For viewing the interface between the Mn_3O_4 octahedrons and the Ag matrix, the Ag crystal is tilted in the ⟨110⟩ zone axis. For the Mn_3O_4 precipitates this results in two distinct situations owing to the difference between the *a*- and the *c*-axis, i.e. ⟨110⟩ (1/3 probability) and (near to) ⟨101⟩ (2/3 probability). The distinction can easily be observed in HRTEM images using the Ag crystal as reference. In the ⟨110⟩ Ag zone axis the octahedron is projected into a lozenge (with two equal sharp and two equal blunt angles). At the sharp tip the precipitate thickness reduces to zero and no analysis is possible. At the blunt corner the precipitate thickness is maximum and suffers least from Moire effects (which often still can remain a problem due to the small size of the Mn_3O_4 precipitates in Ag, but which can be circumvented by only analysing precipitates in sufficiently thin parts of the foil). This blunt corner corresponds to an angle of 117.1° in the case of ⟨110⟩ Mn_3O_4 and to 105.8° in case of ⟨101⟩ Mn_3O_4, whereas the corresponding angle between {111} planes in a cubic crystal such as Ag is 109.5°; ⟨101⟩ Mn_3O_4 is shown in Fig. 1, where it can be seen that the blunt angle between the {111} planes of Mn_3O_4 is smaller than between the ones of Ag. Some HRTEM images with ⟨110⟩ Mn_3O_4 zone axis will be shown below, which are more interesting than with ⟨101⟩ Mn_3O_4, because the *c*-axis which contains all significant mismatch with Ag is in that case in the plane of projection. Moreover, parallelism of principal axis implies that ⟨101⟩ Mn_3O_4 is not parallel to ⟨101⟩ Ag and an in-between angle of 4.16° occurs. Hence, if the Ag crystal is tilted as accurately as possible in the ⟨110⟩ zone axis, the interfaces between Mn_3O_4 and Ag are in the case of ⟨101⟩ Mn_3O_4 not viewed end-on and analysis of the atomic structure of the interface should then not be performed.

The tilt between the eight {111} facets of Mn_3O_4 and the {111} planes of Ag in the case of parallelism of principal axis is 3.83° (with [110] or [1$\bar{1}$0] as the tilt axis). For a tilt with this magnitude, ledges (in the metal) with [110] or [1$\bar{1}$0] direction along all faces of the octahedron can be expected. For the 3.83° tilt ledges on, for example, the (1$\bar{1}$1) face with direction [110] and height 1/4[1$\bar{1}$2] can be expected each 14 1/4[$\bar{1}$12] (i.e. for each 14 ($\bar{1}$11) planes) and the corresponding projection to be expected for viewing in the [110] direction is shown schematically in Fig. 3(a). The HRTEM image shown in Fig. 4 for viewing in the [110] direction corresponds well to the expected situation. The two {111} planes in the projection make an angle at the blunt corner which is clearly larger for Mn_3O_4 than for Ag (117.1° vs 109.5°) and the misalignment and hence "ledges" occur at each of the two {111} facets pairs in the projection. The distance between the "ledges" along the interface as can be observed in Fig. 4 is 14 and

twice 11 1/4⟨112⟩, the last being near to, but somewhat smaller than the expected distance of 14 1/4⟨112⟩. A smaller distance between the ledges is expected if the height of the ledges is less than a full 1/4⟨112⟩ step. This is often the case and will be considered in more detail below (Section 3.4). Local

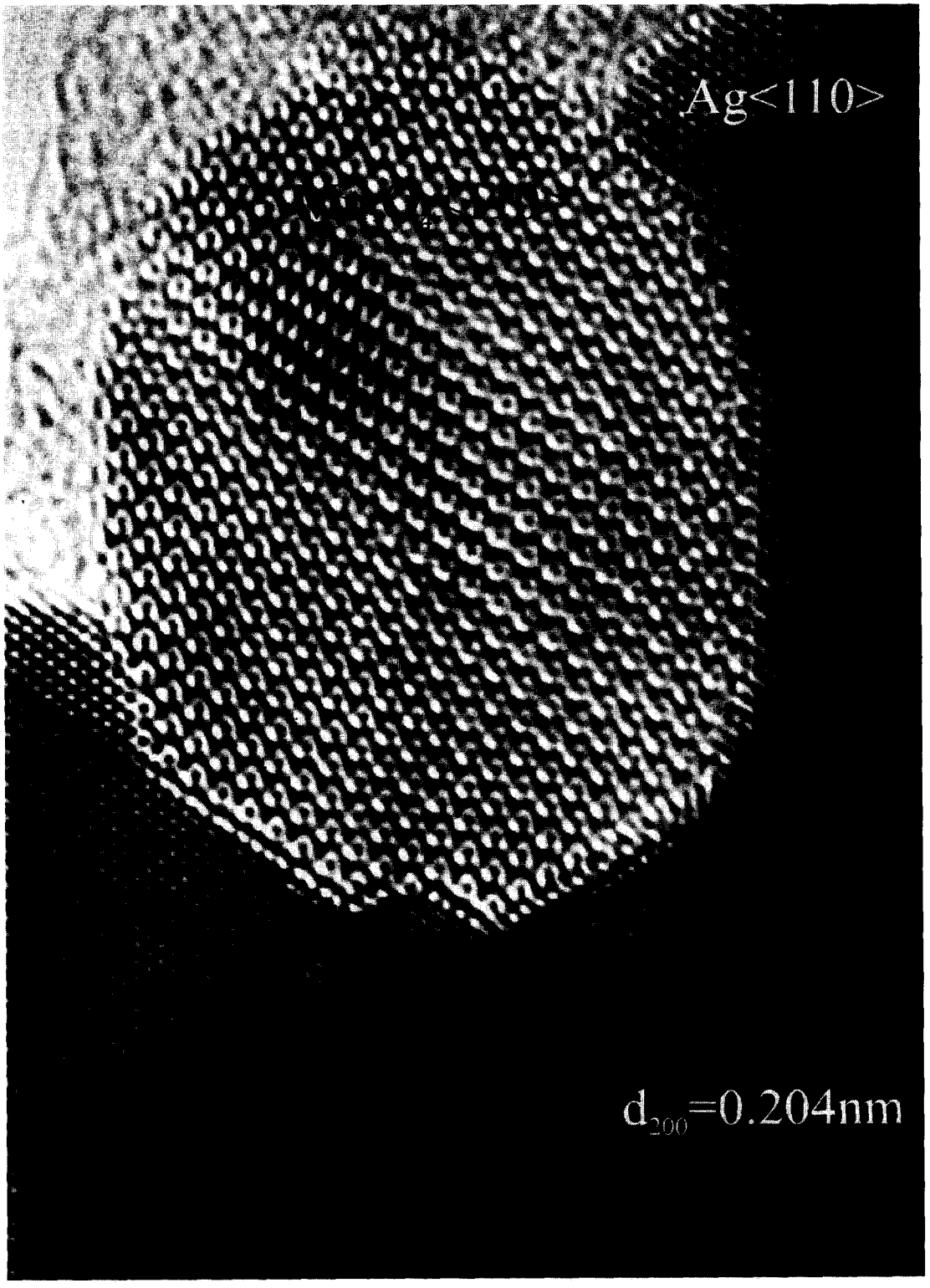

Fig. 2. HRTEM image of an Mn_3O_4 precipitate with a relative large (001) facet in Ag; viewing direction along the common ⟨110⟩ of Mn_3O_4 and Ag.

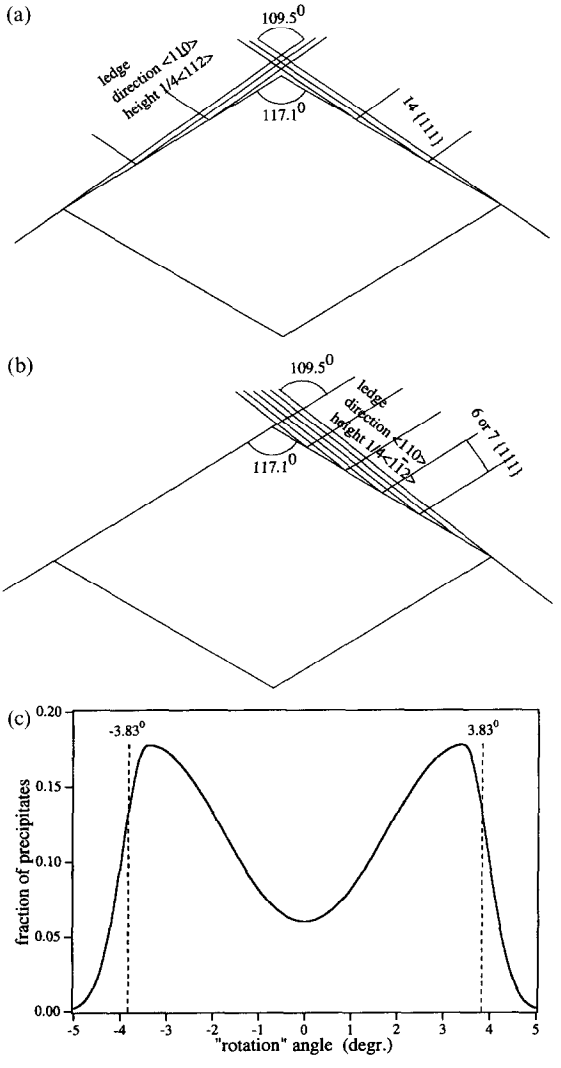

Fig. 3. Schematic representation of a Mn_3O_4 precipitate with an octahedron shape due to {111} facets in Ag as seen when projected along the common ⟨110⟩ of Mn_3O_4 and Ag (a) with an equal tilt of 3.83° present on all interfaces, (b) with a parallel and a 7.67° tilted pair of interfaces. (c) The qualitative dependence between the fraction of Mn_3O_4 precipitates and the rotation they possess with respect to the alignment with parallel principal axes of Mn_3O_4 and Ag.

plane bending in Ag (and as expected to a lesser extent in Mn_3O_4), however, may reduce the tilt of 3.83° and thus increase the distance between ledges to be expected. The short facets of the Mn_3O_4 precipitates in Ag are not ideal for analysis of periodic features along the interface. However, a big advantage of Mn_3O_4 in Ag is that the mismatch along the interface is essentially one dimensional and can thus be perpendicular to the viewing direction keeping the atomic columns in the viewing direction straight (in contrast with the bent columns in the case of the two-dimensional mismatch at Cu/MnO interfaces, as will be considered in Ref. [2]).

The situation where misalignment and ledges are present on all eight {111} facets as shown in Fig. 4 is not so frequently encountered. Both SAED (cf. Fig. 1 for the faint splitting of the (400) Mn_3O_4 spots) and HRTEM (see below) show that most octahedrons tend to be rotated, with approximately 3.8° around [110] (or [1$\bar{1}$0]), with respect to the matrix, to bring {111} faces in Ag and Mn_3O_4 parallel for a pair of facets. Then, at another pair of facets the {111} planes of oxide and metal become less aligned. The theoretically expected projection for this situation, for viewing in the [110] direction and with the rotation axis parallel to the viewing direction, is shown schematically in Fig. 3(b). The experimental HRTEM image corresponding to this situation is shown in Fig. 5. In this case (with 1/6 probability) the [110] Mn_3O_4 is still parallel to the [110] Ag, whereas in all other cases the [1$\bar{1}$0] or ⟨101⟩ of Mn_3O_4 are not parallel to the corresponding directions of Ag. It can be clearly seen in the projection of Fig. 5 that one pair of facets corresponds to parallel {111} planes and the other pair of facets corresponds to tilted {111} planes showing several ledges. Theoretically a tilt of 7.67° is expected for the non-parallel {111} interface. Then on, for example, the (1$\bar{1}$1) face ledges with direction [110] and height 1/4[1$\bar{1}$2] can be expected theoretically each 6.67 1/4[$\bar{1}$12] [i.e. for each 6.67 ($\bar{1}$11) planes; cf. Fig. 3(b)]. In the experimental image the separation between the three ledges observed on each of the two facets is 7 ± 1 1/4⟨112⟩, which agrees well with the expected distance (to have a more detailed view of the repeat distance between the ledges, see Fig. 11 below).

Analysis of the "rotation" of Mn_3O_4 with respect to the Ag crystal for a large number of precipitates indicates that the rotation is not discretely 0° or ± 3.83° but exhibits a continuous distribution, which corresponds qualitatively to the one shown in Fig. 3(c). Probably, the exact parallelism of {111} planes in oxide and metal does not determine the rotation directly, but the degree of parallelism necessary to result in a pair of facets without ledges and this is also possible when small deviations from ±3.83° occur. This leads to the conclusion that a tendency exists to align {111} planes nearly parallel in oxide and metal for one pair of facets in such a way that no ledges have to be present on this pair of facets.

3.3. *Parallel {111} interfaces*

An experimental HRTEM image showing in detail an Ag{111}//Mn_3O_4{111} interface as viewed along [1$\bar{1}$0] is presented in Fig. 6(a). The mismatch between Mn_3O_4 and Ag at this interface is basically a mismatch of 10.4% in the [11$\bar{2}$] direction only (i.e. neglecting the mismatch of −0.4% in [1$\bar{1}$0]). Hence, an advantage of the Ag/Mn_3O_4 system is that the mismatch along the interface is one dimensional, which is likely to give an array of misfit dislocations which can be observed end on in HRTEM images.

Usually a two-dimensional network of misfit dislocations at semi-coherent metal/oxide interfaces is present, which relieves the mismatch present along all directions in the interface plane. In HRTEM images this 2-D network is then projected along 1-D, making unambiguous interpretation hardly possible.

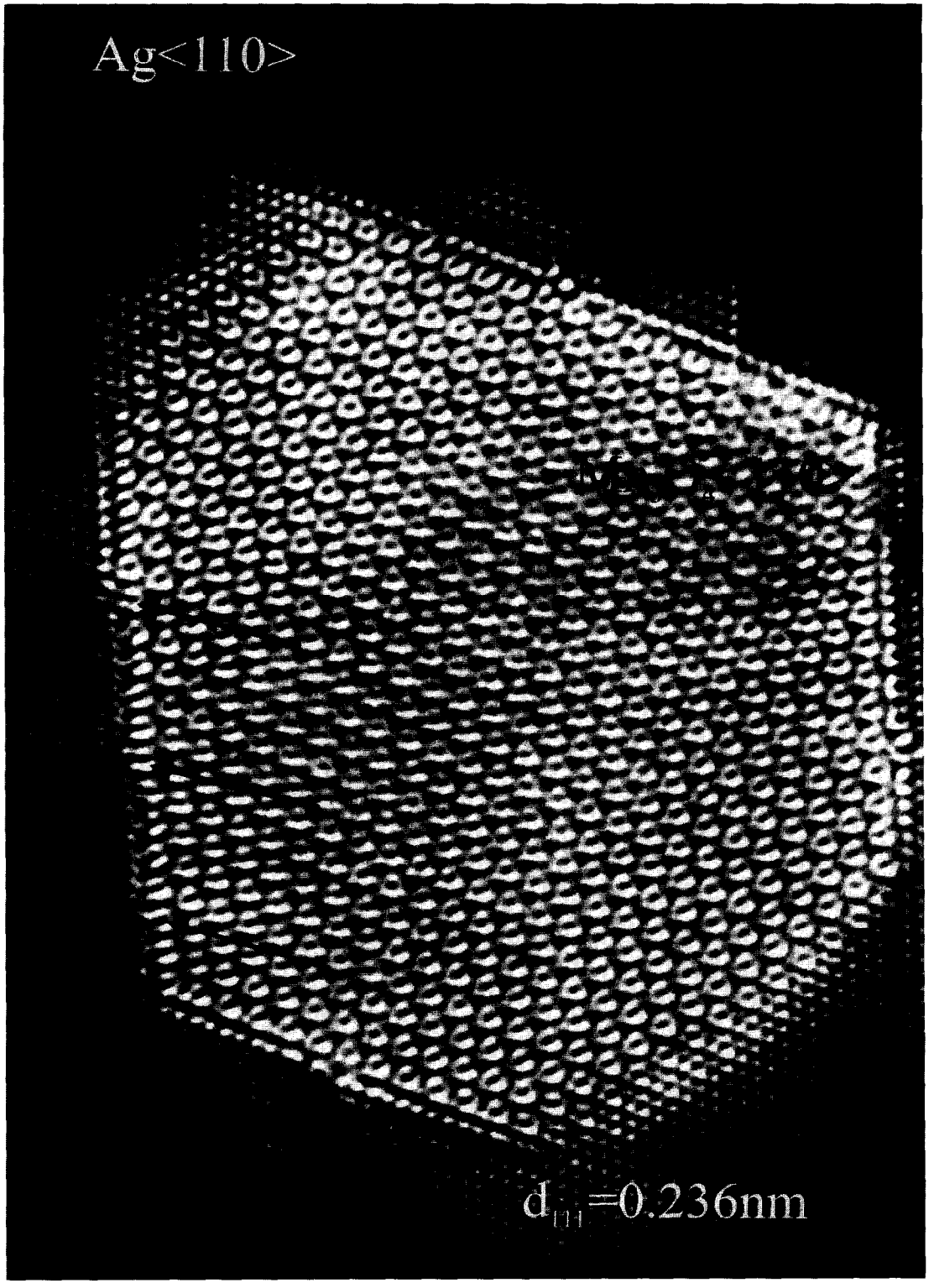

Fig. 4. HRTEM image of an Mn_3O_4 precipitate in Ag as seen when viewed along the common ⟨110⟩ of Mn_3O_4 and Ag showing a nearly equal tilt of 3.8° on all interfaces, which is relieved by ledges in the Ag along the ⟨110⟩ with height 1/4⟨112⟩ (the third index may not be permuted, because it is fixed by the *c*-axis of Mn_3O_4).

See, for instance, Ref. [2], which shows the difficulty of interpreting the network of misfit dislocation at interfaces with parallel {111} planes for the Cu/MgO [9–12], Pd/MgO [12], Cu/MnO [8, 1] and Ag/CdO [13] systems as either a hexagonal network (Burgers vector 1/2⟨110⟩, line direction ⟨112⟩) or a trigonal

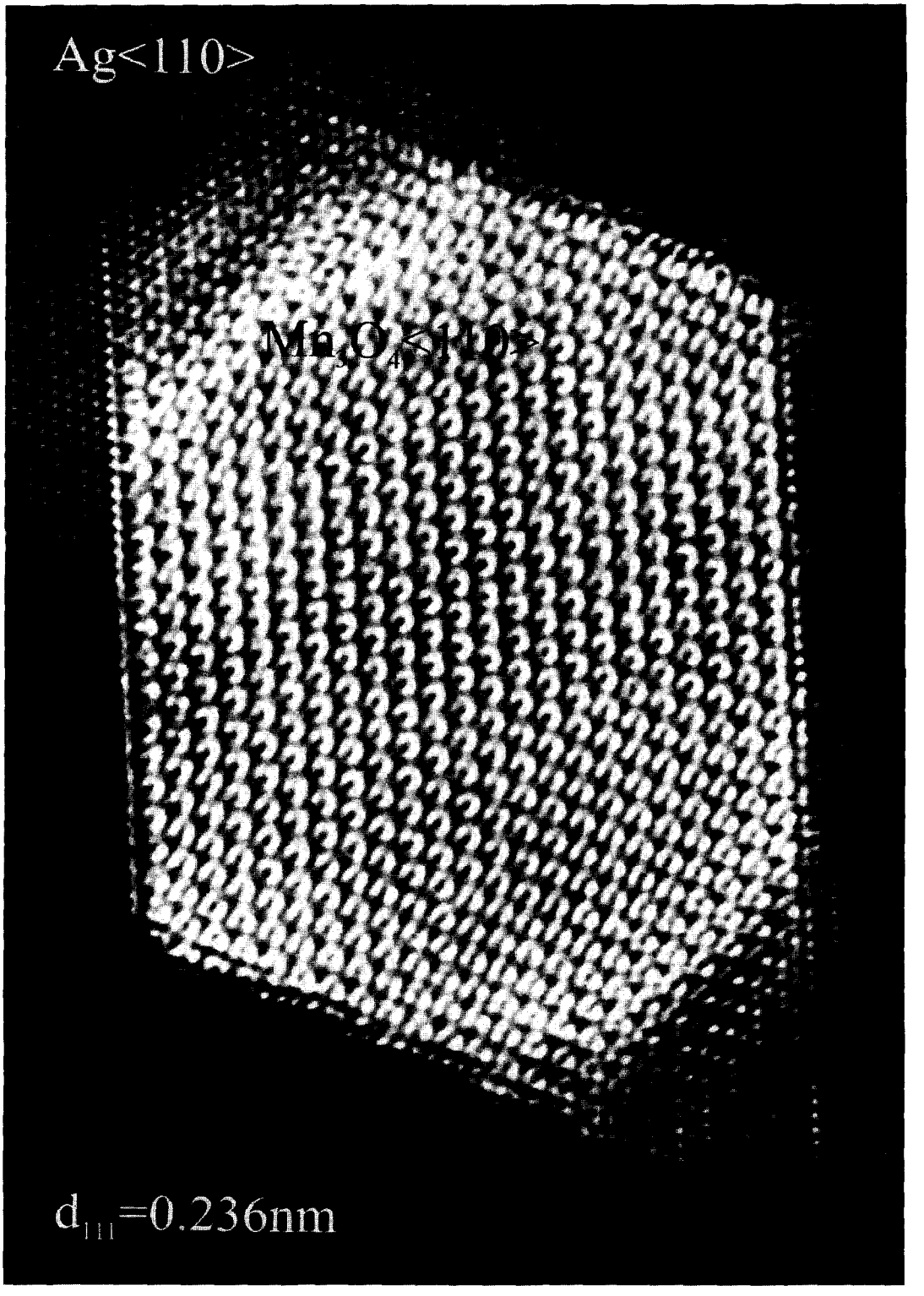

Fig. 5. HRTEM image of an Mn_3O_4 precipitate in Ag as seen when viewed along the common ⟨110⟩ of Mn_3O_4 and Ag showing a parallel and a 7.6° tilted pair of interfaces; the tilted interfaces exhibit ledges in Ag along the ⟨110⟩ with height 1/4⟨112⟩ (the third index may not be permuted, because it is fixed by the *c*-axis of Mn_3O_4).

network (Burgers vector 1/6⟨112⟩, line direction ⟨110⟩). A disadvantage of the Ag/Mn_3O_4 interface, besides its relatively short length, is that direct observation of misfit dislocation cores with localized plane bending separating coherent-interface regions in the HRTEM image is difficult because Mn_3O_4 does

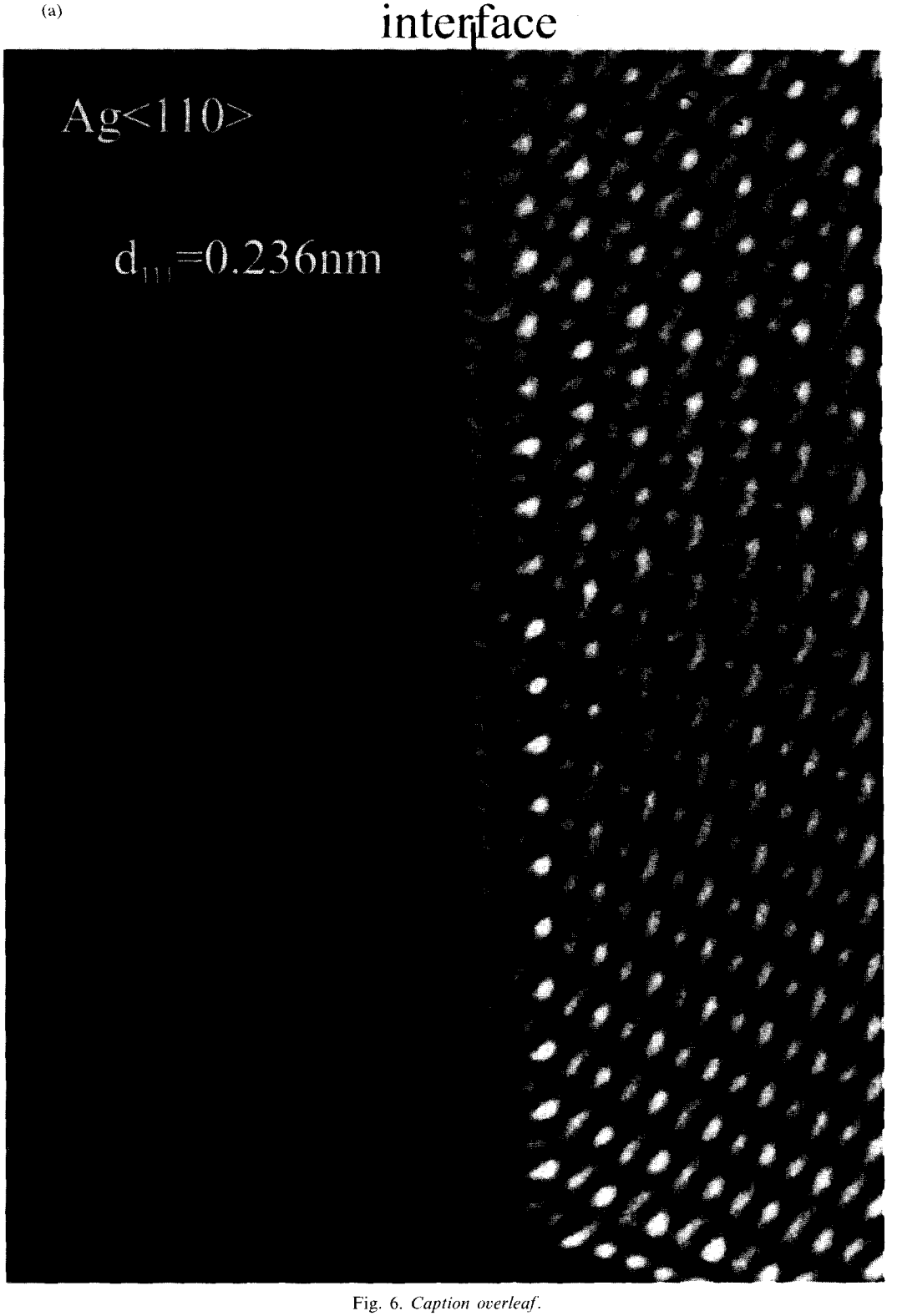

Fig. 6. *Caption overleaf.*

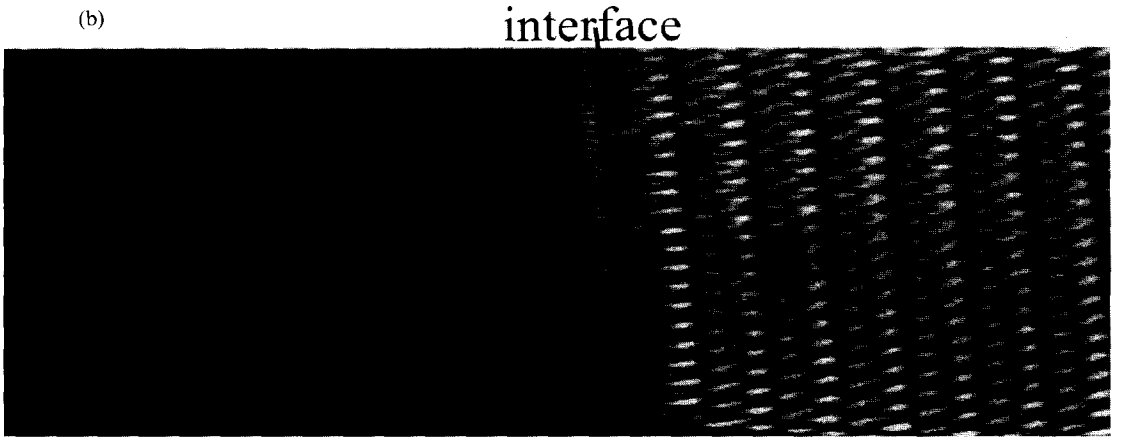

Fig. 6. (a) HRTEM image of a parallel $\{111\}$ Ag/Mn_3O_4 interface viewed along the common $\langle 110 \rangle$ of Mn_3O_4 and Ag. Bright dots in Ag correspond to the position of atomic columns. Viewing the image along the interface under grazing angle undulations can be observed primarily in between the Ag planes most near to the interface. (b) The same image as in (a) but contracted by a factor of 3 along the interface; solid-lined arrows indicate the position of $1/3[11\bar{2}]$ Burgers vectors at the interface and dashed-lined arrows $1/6[11\bar{2}]$ Burgers vectors.

not show a simple direct correspondence to the atom positions (e.g. with black or white dots). However, another effect of the mismatch at the Ag/Mn_3O_4 interface can still be observed (with some difficulty) directly. Viewing along the interface in the image under acute angle, the Ag$\{111\}$ planes nearest to the interface are not straight parallel to the interface, but show a periodic undulation. In particular the dark region in between the first and second Ag$\{111\}$ planes parallel to the interface (atomic columns are imaged as bright dots) becomes periodically wider and smaller along the interface. The period of this undulation along the interface corresponds to 10 ± 1 $1/4[11\bar{2}]$ Ag and thus correlates well with the mismatch present along $[11\bar{2}]$ of the Ag/Mn_3O_4 interface. To make the existence of these wavy $\{111\}$ Ag planes clearer the glancing-angle view is mimicked in Fig. 6(b) by contracting the image parallel to the interface by a factor of 3.

In order to be able to interpret these undulations in terms of a misfit-dislocation structure, atomistic (lattice statics) calculations were performed which subsequently were used as input for HRTEM image simulation. Based on the mismatch at the Ag/Mn_3O_4 system a dislocation array with line direction $[1\bar{1}0]$ (i.e. only the ones perpendicular to the c-axis of the distorted spinel) and Burgers-vector direction $[11\bar{2}]$, if possible all of type $1/6[11\bar{2}]$ is expected. The atomistic calculations, determining the relaxed configuration of Ag atoms adjacent to an assumed rigid tetragonal–distrotated f.c.c. structure, which mimics Mn_3O_4, were performed for the correct interface geometry/crystallography and a mismatch of 10% in the $[11\bar{2}]$ (i.e. 11 periods in the metal vs 10 periods in the oxide in this direction) and no mismatch in the $[1\bar{1}0]$. Also in the $[1\bar{1}0]$ the block of atoms is taken sufficiently large (i.e. 11 periods in the metal *and* the oxide) to avoid a one-dimensional result which was imposed by boundary conditions a priori. The oxide is approximated with a mono-atomic basis. These "effective" atoms can best be regarded as coincident with the oxygen atoms. The program used is described in detail in Refs [5] and [15]. The interaction functions between the Ag atoms are of the Finnis–Sinclair type [16]. The interaction between metal and oxide across the interface is described phenomenologically by αV_{eff} with V_{eff} the effective pair potential for Ag based on the many-body Finnis–Sinclair potential [17] and α a factor allowing simulation of different interaction strengths over the interface. The mismatch used in the simulations can be taken close to the real mismatch under the restriction that commensurate blocks of atoms are taken for the metal and the oxide. The relaxed structure for $\alpha = 2$ is shown in Fig. 7(a) for viewing in the $[1\bar{1}0]$ direction and in Fig. 7(b) for viewing along the interface normal [111], with the positions of the oxygen atoms in the terminating oxygen layer at the interface as small black dots and the position of the Ag atoms at the interface as larger dots with different grey levels. The darker the Ag atoms the smaller the distance from these Ag atoms to the (planar) interface plane. In Fig. 7(c) the Burgers-vector distribution based on the disregistry between the position of the oxygen atoms and of the Ag atoms in the first layer on each side of the interface is shown, together with the distance between these Ag atoms and the first (111) plane of the oxide. The results can be interpreted as an array of edge dislocations with line direction $[1\bar{1}0]$ and alternating $1/6[11\bar{2}]$ and $1/3[11\bar{2}]$ Burgers vector and apparently the mismatch cannot be relieved by Shockley partials only, and although a two-dimensional network of dislocations could have formed, a one-dimensional array appeared to be more favourable. The most favourable position of the Ag atoms at the interface with respect to the oxide is in the hollow sites with

Ag above a triangle of oxygen atoms. (This is also the geometry used in recent *ab initio* calculations on the polar Cu(111)//MgO(111) interface [14].) The Burgers vector $1/3[11\bar{2}]$ is located in the middle between two such favourable sites with the Ag atom directly on top of an oxygen atom (least-favourable site). The Burgers vector $1/6[11\bar{2}]$ is also located in the middle between two favourable three-fold oxygen co-ordinated sites, but now the Ag atom has 2 nearest neighbouring oxygen atoms. The distance between the Ag atoms and the first (111) plane in the oxide clearly reflects these co-ordinations and thus correlates logically to the Burgers vectors. According to the atomistic calculations shown in Fig. 7, $\{111\}$ Ag planes parallel and near to the interface clearly show undulations, also observed in Fig. 7(a) best under acute angle, which should be resolvable by HRTEM and probably resolved in the experimental image of Fig. 6.

The Burgers vectors which are present according to the atomistic calculations separate alternating regions with, according to the f.c.c. structure, correct stacking over the interface and with a stacking fault at the interface. Ag has a low stacking fault energy [18] and therefore the occurrence of the stacking faulted regions seems natural. However, stacking faults are only present when considering the stacking over the interface and the (unfounded) use of the effective pair potential for Ag to describe the interaction across the interface may have unjustly led to the introduction of these stacking faults. An important point in this respect is that *ab initio* calculations for metal/ceramic interfaces indicate that the interaction over the interface is short range and predominantly confined to first nearest-neighbour interaction. This was shown in several studies on non-polar (100) interfaces [19, 20], but now also recently for the polar Cu(111)//MgO(111) interface [14]. Since the first nearest-neighbour co-ordination is identical for f.c.c. and c.p.h. stacking it is probable that the energy difference between these two kinds of stacking is small. Therefore the present results still appear appropriate. Apart from theoretical arguments the comparison of the calculated relaxed structure with the experimentally observed one is of course more decisive.

MacTempas calculations [3] were performed for the above relaxed atomic structure of the Ag(111)// Mn_3O_4(111) interface. The mono-atomic oxide lattice used in the above calculations was then replaced by the Mn_3O_4 lattice, with the oxygen atoms of Mn_3O_4 taken coincident with the mono-atoms. The resulting image simulation is shown in Fig. 7(d) for a sample thickness of 4 nm, which is thought to be near to the experimental situation pertaining to Fig. 6, a defocus of -6 nm (known with reasonable accuracy from experiment) and a beam tilt of 1.3 mrad. A beam tilt can be expected since a voltage-centre alignment and not an axial coma alignment was performed before obtaining the experimental images. The experimental

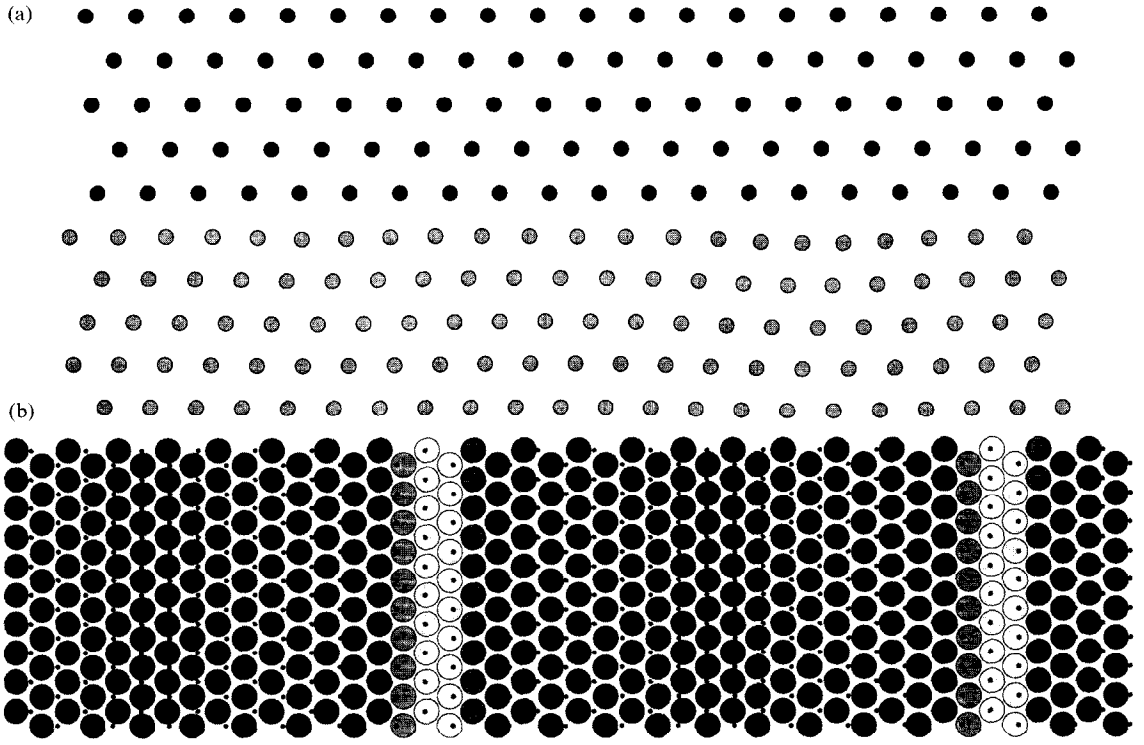

Fig. 7. *Caption overleaf.*

(c)

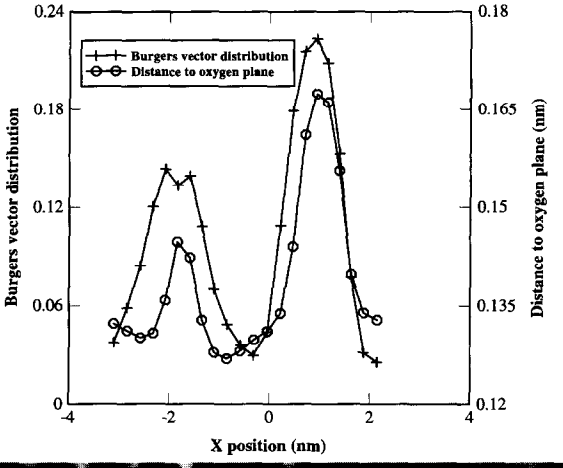

(d)

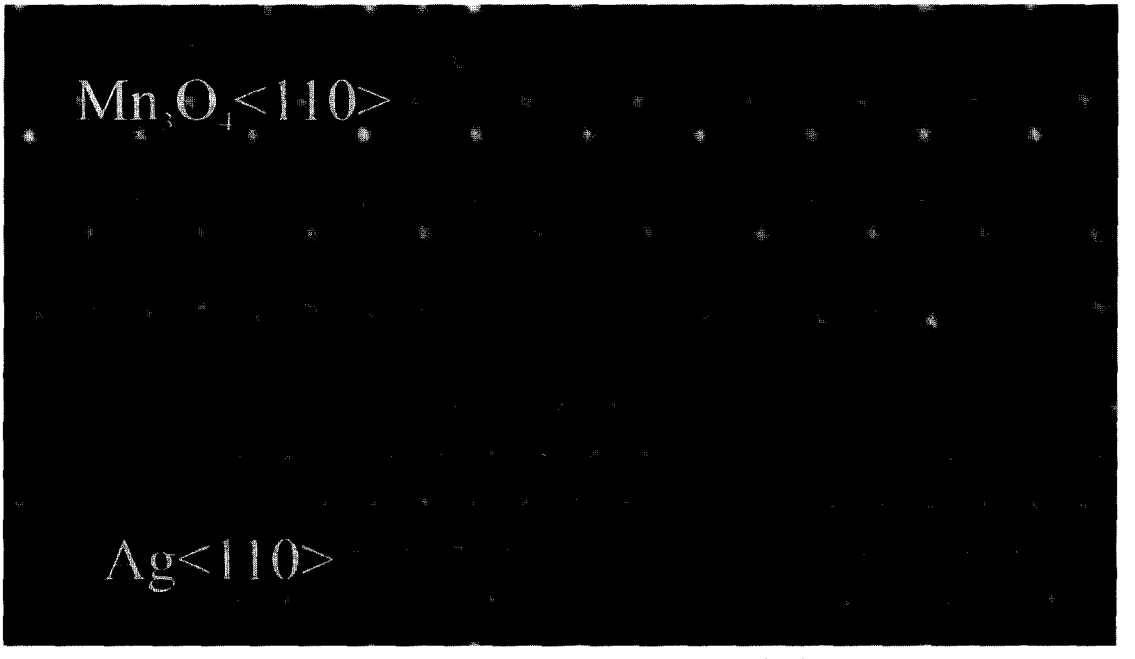

Fig. 7. Relaxed structure (results of atomistic calculations) for the parallel $\{111\}$ Ag/Mn_3O_4 interface with mismatch of 10.0% (11 periods in the metal vs 10 in the oxide) only along the $[11\bar{2}]$ direction in the interface. The factor α allowing simulation of different interaction strengths across the interface was given a value 2. (a) View along the $[1\bar{1}0]$ with edge-on observation of the interface; black dots denote the oxygen atoms and shaded dots the Ag atoms. (b) View along the interface normal [111]. Small black dots denote the oxygen atoms in the terminating layer of the oxide and larger dots with different grey levels denote the Ag atoms in the first layer at the interface; the darker the indication of the Ag atoms the smaller the distance between the Ag atoms and the planar interface. (c) The Burgers vector distribution based on the disregistry between the position of the Ag atoms and the position of the oxygen atoms along the interface (open dots) and the distance between the Ag atoms and the planar oxygen layer terminating the oxide (crosses). (d) Simulated HRTEM image (MacTempas) of the parallel $\{111\}$ Ag/Mn_3O_4 interface using the relaxed structure as input for the simulation. View along the common $\langle 110\rangle$ of Mn_3O_4 and Ag, defocus -6 nm, thickness 4 nm and a beam tilt of 1.3 mrad; the bright dots in Ag correspond to atomic columns.

HRTEM images were simulated best if the Mn_3O_4 was terminated by a close-packed oxygen plane followed by a close-packed manganese plane.

The undulations are still clearly present in Fig. 7(d) and comparison of Figs 6 and 7(d) indicates that the atomistic calculations give a fair explanation for the experimentally observed undulations at the $Ag(111)//Mn_3O_4(111)$ interface. In order to try to make this comparison quantitative, the distance between the $[1\bar{1}0]$ Ag atomic columns in the second $\{111\}$ plane with respect to the interface and a straight line positioned as correctly as possible at the expected interface plane was extracted from both the experimental and simulated HRTEM images [Figs 6 and 7(d), respectively]. The results are shown in Fig. 8 as a function of the distance along the interface ($[11\bar{2}]$) with experimental results in the top figure and the results based on the simulated image in the

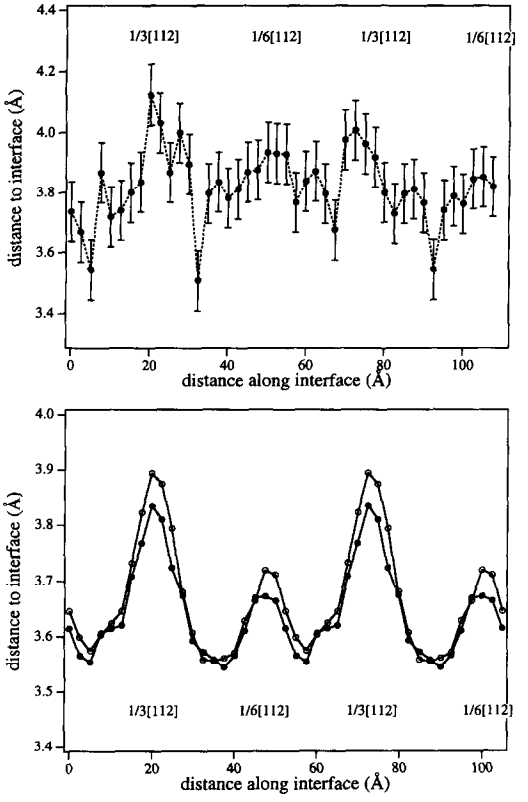

Fig. 8. Distance between the $[1\bar{1}0]$Ag atomic columns in the second $\{111\}$ layer counted with reference to the interface and the interface plane as a function of the distance along the interface ($[11\bar{2}]$) as based on the experimental HRTEM image of Fig. 6, shown in the top figure, and as based on the simulated image of Fig. 7(d), shown in the bottom figure.

bottom figure. The co-ordinates of the atomic columns were determined by applying a threshold discriminating between black and white and then determining the centres of the white dots corresponding to the individual atomic columns. Two sets of results are shown in the bottom of Fig. 9 corresponding to two different threshold values; the best results are obtained by allowing the white dots in the HRTEM image to be as large as possible but still separate from their neighbours, as was the case for the open dots in the bottom of Fig. 9 [cf. Fig. 7(c)]. The position of the atomic columns as determined with this procedure is rather sensitive to noise and to diminish this sensitivity the experimental image was first smoothed before applying the procedure. The experimental results show the minimum and maximum in the distance from the Ag columns to the interface with mutual separations, i.e. distance along the interface, which correspond reasonably well with the expected ones. In the results based on the simulated image it is (of course) possible to distinguish the Burgers vectors of type $1/3[11\bar{2}]$ and of type $1/6[11\bar{2}]$. In the experimental results it is hard to make this distinction. However, two of the undulations in Fig. 6 corresponding to the first and third maximum in Fig. 8 seem to correspond to stronger distortions in the lattice than the other two and these stronger distortions are ascribed to $1/3[11\bar{2}]$ and the weaker ones to $1/6[11\bar{2}]$; in Fig. 6 the solid-line arrows denote $1/3[11\bar{2}]$, the dashed-line arrows denote $1/6[11\bar{2}]$.

An interesting question is whether the undulations of the $\{111\}$ Ag planes parallel and near to the interface indicate the presence of misfit-dislocation cores. According to the atomistic calculations, undulations only arise if adhesive interaction is present across the interface. If the factor α is set to zero, an incoherent interface with planar $\{111\}$ Ag results and the larger α becomes the more localized the dislocations and the undulations along the interface become. One can still argue that at an incoherent interface, where no localized dislocations are present, the distance from the Ag atoms to the close-packed oxygen layer which terminates the oxide reflects the packing of Ag "spheres" on this oxygen layer, i.e. if by accident an Ag atom is above a hollow side constituted by a triangle of O atoms the distance is short or if the Ag atom is by accident on top of one O atom the distance is large. Then undulations arise which are not connected to misfit dislocations. However, the change of planar $\{111\}$ Ag in waving planes requires energy by interaction across the interface. Owing to the geometry of the interface this interaction will give rise to more and less favourable sites for Ag atoms on the terminating oxygen layer. This interaction then results automatically in the formation of dislocation cores (apart from the possibility that a coherent interface arises) and the strength of the interaction determines the degree of localization. Therefore the observed undulations can be conceived as a direct indication for the presence of dislocation cores.

The Burgers vector of $1/3[11\bar{2}]$ corresponding to an Ag atom directly on top of an oxygen atom is unfavourable and it may be expected that removal of this type of unfavourable Ag atom occurs by climb of the dislocation into the metal, associated with dissociation of the unfavourable Burgers vector into more favourable partials e.g. Shockley's. To verify if this mechanism is realistic, the atomistic calculations were again performed after the unfavourable Ag atoms (a column along $[1\bar{1}0]$) were removed from the starting configuration of the block of atoms to be relaxed. The resulting structure after relaxation is shown in Fig. 9(a) for viewing along $[1\bar{1}0]$ and in Fig. 9(b) for viewing along the inferface normal. In Fig. 9(b) the two $\{111\}$ Ag planes nearest to the interface and the terminating oxygen layer are shown: small black dots denote the oxygen layer; the large dots with different grey levels denote the first Ag$\{111\}$ layer and the largely shielded large dots denote the second Ag$\{111\}$ layer counted with reference to the interface. The different grey levels are a measure of the distance between the Ag atoms in this first layer and the interface; the smaller the distance the darker

the dots. The atomistic calculations give the result that the structure after climb and dissociation of $1/3[11\bar{2}]$ has a lower energy than the original structure shown in Fig. 7 (see Table 1). Some dislocations, however, have shifted from the interface across which pair potentials operate into the Ag in which many-body potentials operate, and this makes the calculated energy difference between both structures less reliable.

Interpreting the atomistic structure shown in Fig. 10 in terms of misfit dislocations shows that the $1/6[11\bar{2}]$ Burgers vector already present in the results shown in Fig. 7 is unchanged. The $1/3[11\bar{2}]$ Burgers vector after climb also effectively becomes a $1/6[11\bar{2}]$ (smeared out in between the oxygen and the second Ag layer) and this is possible because a $1/6[11\bar{2}]$ is emitted parallel to the interface and is localized between the first and second Ag{111}. So, instead of

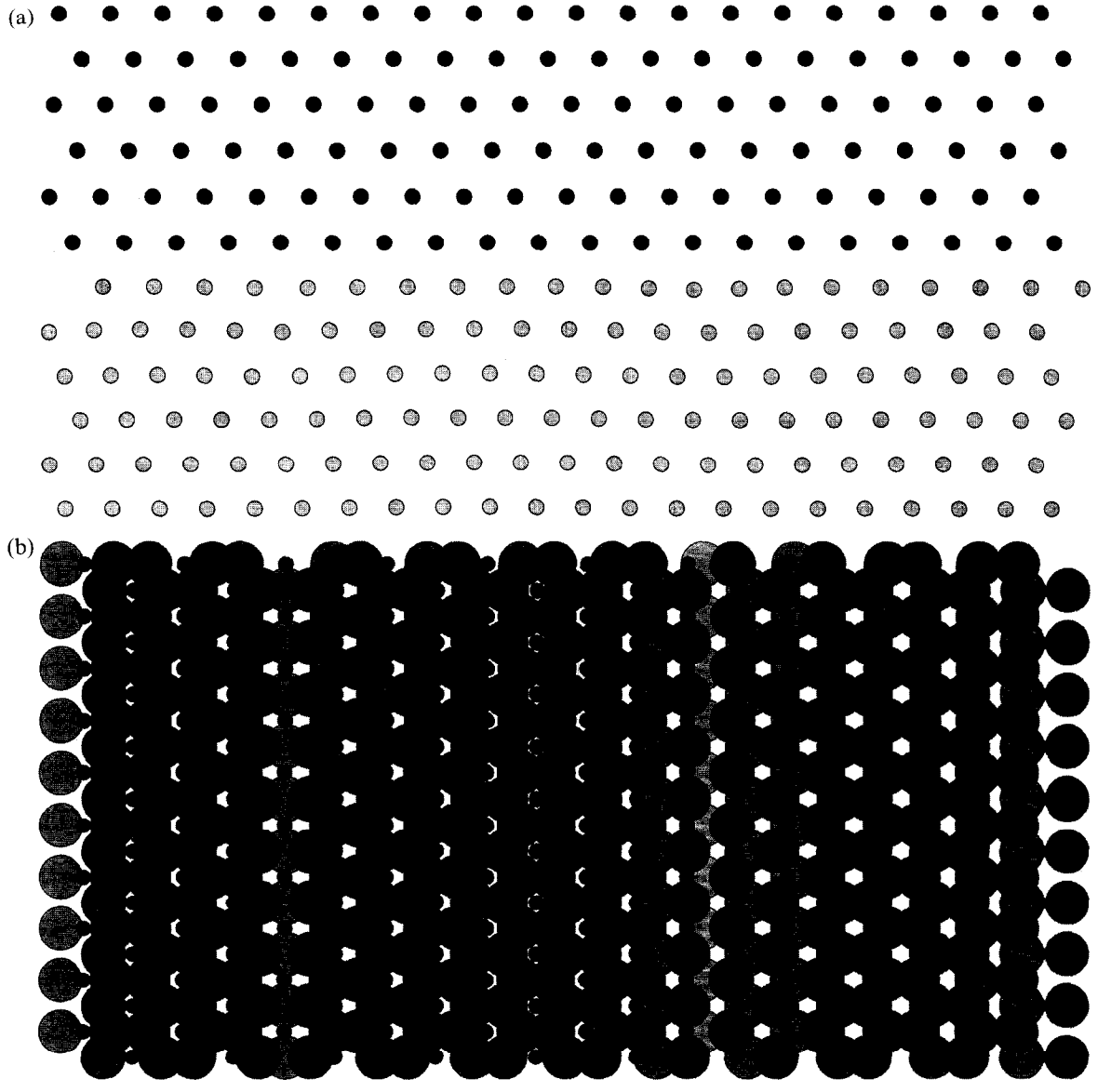

Fig. 9. Relaxed structure (results of atomistic calculations) for the parallel {111} Ag/Mn_3O_4 interface with a mismatch of 10.0% only along the $[11\bar{2}]$ direction in the interface ($\alpha = 2$); a $[1\bar{1}0]$ column of Ag atoms, positioned at the core of the $1/3[11\bar{2}]$ Burgers vector in the results shown in Fig. 7, was removed from the starting configuration to be relaxed to simulate the possible climb and dissociation of the unfavourable $1/3[11\bar{2}]$ Burgers vector. (a) View along the $[1\bar{1}0]$ with edge-on observation of the interface; black dots denote the oxygen atoms and shaded dots the Ag atoms. (b) View along the interface normal [111]. Small black dots denote the oxygen atoms in the terminating layer of the oxide and large dots with different grey levels denote the Ag atoms in the first layer and largely shielded large dots denote the Ag atoms in the second layer from the interface; the darker the indication of the Ag atoms in the first layer the smaller the distance between these Ag atoms and the planar interface.

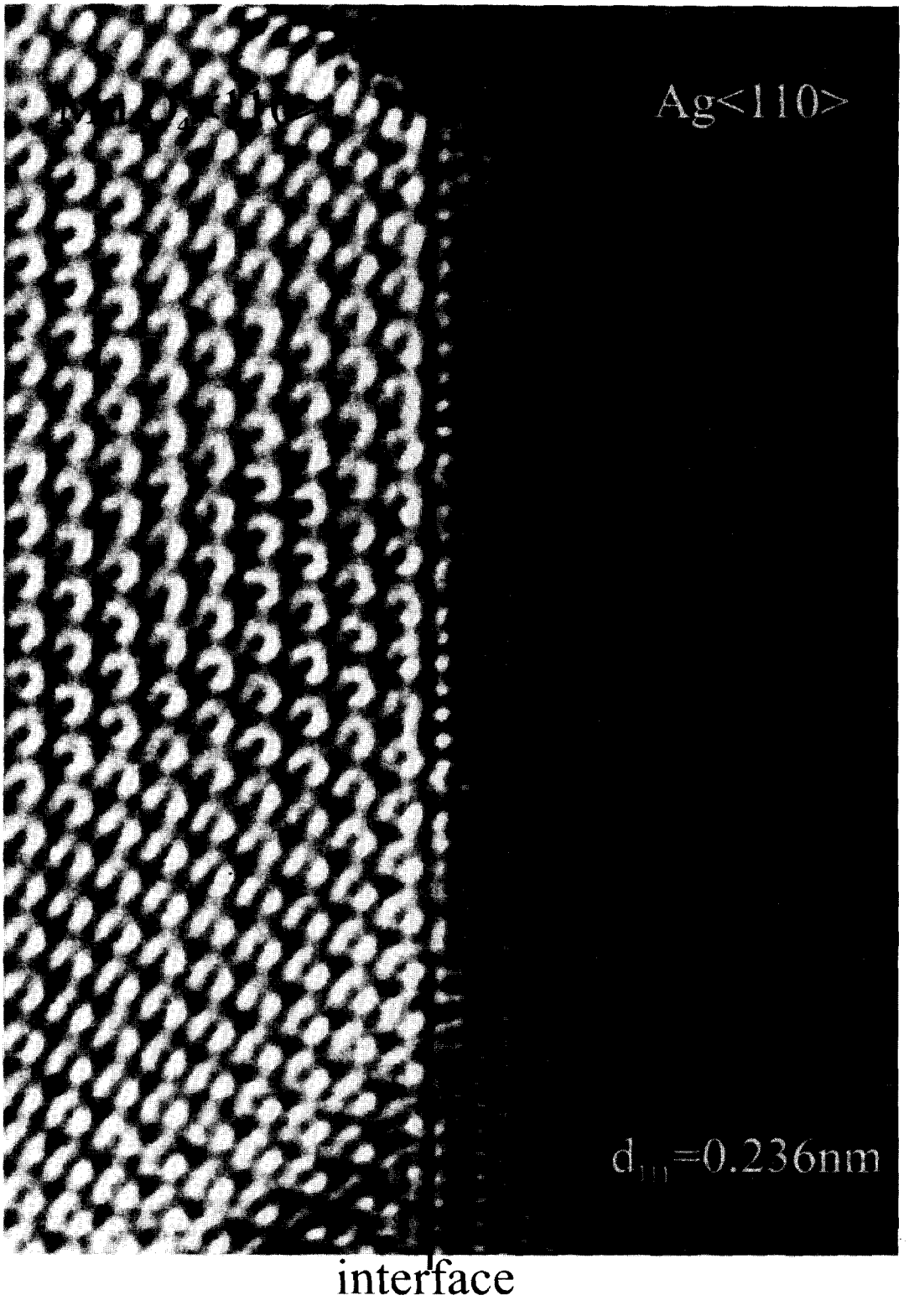

Fig. 10. HRTEM image of a parallel {111} Ag/Mn_3O_4 interface viewed along the common ⟨110⟩ of Mn_3O_4 and Ag; a misfit-dislocation structure with stand-off in Ag can be observed readily by the incorrect stacking it introduces in the Ag. The arrows give an indication for the location of Shockley partials; large arrows denote Shockley partials with Burgers vectors perpendicular to the viewing direction and short arrows denote Shockley's with Burgers vectors 60° inclined to the viewing direction. Dashed lines denote segments of twin boundaries on {111} Ag.

alternating $1/6[11\bar{2}]$ and $1/3[11\bar{2}]$ Burgers vectors localized at the interface, three $1/6[11\bar{2}]$ are now present which alternate their distance to the interface: one at the interface, then one between the oxygen layer and the second Ag layer and then one between the first and second Ag layer. The three $1/6[11\bar{2}]$ separate three regions at the interface: a correctly f.c.c. stacked part, a part containing a single-plane intrinsic stacking fault (locally c.p.h. stacked) and a part containing a two-layer twin (or three-layer twin depending on definition of excluding or including the boundary plane). These three regions can be readily observed in Fig. 9(a).

This rather typical interfacial structure, if it exists, should be observable by HRTEM. There are indeed at present clear indications by experimental HRTEM images that, although not in detail, the type of phenomena described by the atomistic calculations do exist at a minority of the parallel $\{111\}$ Ag/Mn_3O_4 interfaces.

An experimental image of a parallel $\{111\}$ Ag/Mn_3O_4 interface as viewed along $[1\bar{1}0]$ is shown in Fig. 10. The columns of Ag atoms are imaged as white dots (the same conditions apply here as was used for the image simulation in Fig. 8, where the atomic columns of Ag correspond to the white dots) and the bright Fresnel fringe coincides with the first Ag layer. The interpretation of the observed atomic structure is also indicated in Fig. 10: all arrows indicate Shockley partials where the large ones have Burgers vectors perpendicular to the viewing direction and the short ones have Burgers vectors 60° inclined to the viewing direction. All along the interface the first $Ag\{111\}$ layer is coherent with the terminating oxygen layer. Considering the interface from top to bottom first a single-plane intrinsic stacking fault emerges followed by: a two-layer twin, a stacking fault, a perfect Ag lattice up to the interface, a stacking fault, a two-layer twin, a three-layer twin, a two-layer twin and finally a stacking fault. The vanishing of this stacking fault at the end of the interface is not analysed due to the vanishing thickness of the Mn_3O_4. Totally a disregistry of five times $1/4[11\bar{2}]$ Ag (=1.25 nm) is accounted for with the above dislocation structure and with reference to the interface length this is in agreement with the theoretical mismatch of 10.4%.

This interpretation depends on the location of the interface plane between Mn_3O_4 and Ag, which seems arguable. However, the experimental HRTEM images shown in Figs 6, 10 and 11 stem from the same negative and from different interfaces involving the same precipitate, which was in fact shown in total in Fig. 5. In Fig. 6 the location of the interface plane appears clear because the stacking in the Ag is perfect up to the interface and the misfit dislocations are present at the interface plane. The alternative would be that misfit dislocations are present with stand-off *in* the oxide and this seems inconceivable. Also in Fig. 11 the location of the interface is distinct from the tilt which is present at the interface between the $\{111\}$ planes in the Ag and in the Mn_3O_4. From the location of the interfaces in Figs 6 and 11 the location of the interface in Fig. 10 can be deduced with reasonable confidence. A difference in contrast between the first and second $\{111\}$ Ag layer near the interface is present, which corresponds with the expectation that the bright Fresnel fringe for the underfocus used coincides with the first $Ag\{111\}$ layer and is an additional indication for the location of the interface plane.

When the observed dislocation structure in Fig. 10 is compared with the one predicted with the atomistic calculations (cf. Fig. 9), at first sight similarities can be discerned: e.g. Shockley partials are present with varying distance to the interface and the three different regions predicted by atomistic calculations are also observed experimentally (correct f.c.c. stacking, stacking fault, twin). However, more careful analysis exhibits important differences between calculation and experimental observation. A first difference which is interesting and not a principal one in respect that it discounts the calculated dislocation structure is the coherent first $\{111\}$ Ag layer at the interface seen experimentally. This only shifts the dislocation structure one layer further into the metal and can thus be considered as a "stand-off" of the misfit dislocation cores [21]. A principal difference is that in the calculations effectively three $1/6[11\bar{2}]$ Burgers vectors are present in one period compared to two $1/6[11\bar{2}]$ and, for example, one $1/6[\bar{1}2\bar{1}]$ and one $1/6[2\bar{1}\bar{1}]$ in the experiment. In the experiment at a certain distance to the interface one $1/6[11\bar{2}]$ together with another 60° rotated Shockley can be conceived as a dissociated $1/2[01\bar{1}]$ or $1/2[10\bar{1}]$ and their appearance in Ag is natural, although their separation as governed by the interface appears to be very different from the equilibrium one in bulk Ag and not constant. The dissociation of one $1/3[11\bar{2}]$ Burgers vector into three Shockley's in Ag is according to Frank's rule, excluding the effect of the stacking fault energy, energetically favourable. The dissociation of one $1/3[11\bar{2}]$ Burgers vector in two $1/6[11\bar{2}]$ according to the atomistic calculations would be even more favourable, but involves climb for which diffusion of Ag atoms is necessary, which may hinder the occurrence of this dissociation reaction.

The relatively large difference in dislocation structure at the parallel $\{111\}$ Ag/Mn_3O_4 interfaces as observed experimentally (cf. Figs 6 and 10) is probably in the first instance related to the stand-off of the dislocation cores from the interface. In absence of stand-off the $1/3[11\bar{2}]$ Burgers vector is stable at the interface, whereas with stand-off in Ag this Burgers vector becomes unstable and dissociates. The anomaly that at some interfaces a stand-off of the misfit dislocations is observed and at others a stand-off is not observed is considered in more detail in the next section.

3.4. *Tilted {111} interfaces*

A detailed view of a 7.6° tilted {111} Ag/Mn_3O_4 interface showing several ledges is presented in Fig. 11. The columns of Ag atoms are imaged as white dots and the bright Fresnel fringe has shifted to give mainly bright dots on the first Ag{111} plane. Ledges with direction ⟨110⟩ and step-vector $1/4\langle 1\bar{1}2\rangle$ in Ag at the $\{1\bar{1}1\}$ interface with Mn_3O_4 can be considered a result of the insertion or removal of an extra close-packed half-plane (i.e. only on the Ag side) and thus as a perfect lattice dislocation in f.c.c. (1/2[110]) or as a Frank partial (1/3[111]) depending on whether or not the dislocation separates along the interface a region, which, according to the f.c.c. structure, is correctly stacked perpendicular to the interface from a region showing a stacking fault (locally c.p.h. stacked). If in the case of a Frank partial the stacking fault occurs at the interface in between metal and oxide, this is difficult to detect, because the stacking over the interface between oxide and metal is blurred by the semi-coherent nature of the interface (in the case of incoherence, correlation in stacking over the interface becomes absent) and by the complex HRTEM image, not showing individual atomic columns, of Mn_3O_4. Therefore, it was often not possible to distinguish the ledges as either perfect lattice dislocations or Frank partials. However, if in the case of a Frank partial the stacking fault occurs between the first and second Ag close-packed layer (counted with reference to the interface), detection is more easy. This is not only a hypothetical possibility as is indicated by the observation above of a stand-off of misfit dislocations at the parallel {111} Ag/Mn_3O_4 interface (cf. Fig. 10). And indeed such Frank partials are present in Fig. 11: considering the stacking along the {111} Ag making the large angle with the interface, the last Ag atom (in the principle column) before the step in the first Ag plane is stacked in between two Ag atoms of the second Ag plane. Along the whole length of the tilted interface the first Ag{111} shows a stacking fault with the second one, and from the second to the fourth ledge viewing the interface from left to right the second Ag{111} also shows a stacking fault with the third one. All these Ag atoms (columns) in stacking-faulted position are indicated in Fig. 11 by small black dots in the larger bright dots. In the case where both the first and second Ag{111} planes at the interface are in stacking fault, the Ag exhibits a twin layer at the interface. The same effect of a twinned Ag layer at the interface was also observed above at a parallel {111} Ag/Mn_3O_4 interface (cf. Fig. 10). There a coherent Ag{111} layer at the interface was observed and here also, apart from the Frank partials which account for the tilt,

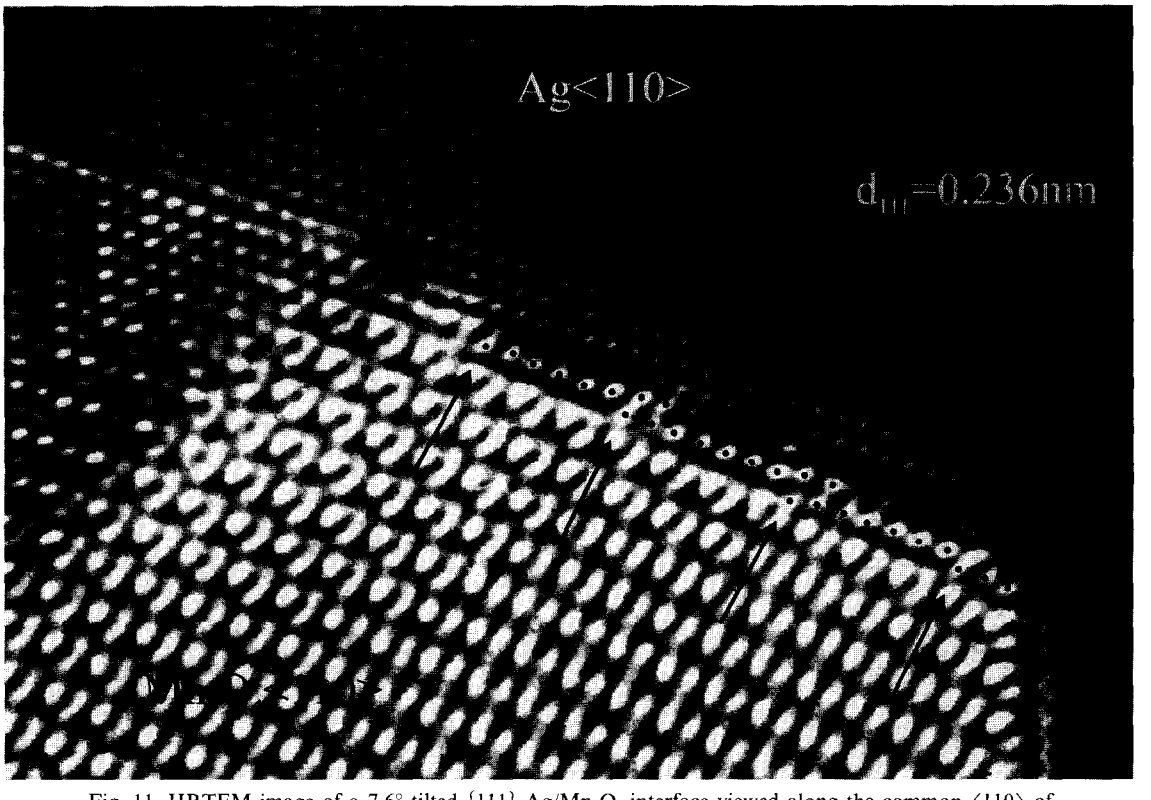

Fig. 11. HRTEM image of a 7.6° tilted {111} Ag/Mn_3O_4 interface viewed along the common ⟨110⟩ of Mn_3O_4 and Ag; a misfit-dislocation structure with stand-off in Ag can be observed readily by the incorrect stacking it introduces in the Ag. The small black dots in the larger bright dots corresponding to the atomic columns indicate atoms in stacking-faulted position. The ledges indicated by arrows can be conceived as Frank partials with Burgers vector perpendicular to the viewing direction.

the Ag{111} layer at the interface is coherent with the terminating oxygen layer of the Mn_3O_4 (this coherence can best be observed by viewing perpendicular to the Mn_3O_4 facet). The mismatch between this first coherent Ag layer and the Ag at a greater distance from the interface is accounted for by the stacking faults present in between the first three Ag layers at the interface. The Frank partials accounting for the tilt are an integral part of the dislocation structure (probably moreover mainly consisting of Shockley partials) accounting for the mismatch along the interface between Ag and Mn_3O_4.

At parallel {111} Ag/Mn_3O_4 two types of interfacial dislocation structure were observed: dislocation cores at the interface (cf. Figs 6–8) and with a stand-off in Ag giving coherence at the interface (cf. Fig. 10). Analogous observations hold for the tilted {111} Ag/Mn_3O_4: Fig. 11 shows a dislocation structure with a stand-off in Ag, but also tilted interfaces were observed where the Ag is stacked perfectly up to the interface and where the mismatch along the interface and of the tilt is completely localized at the interface. Apparently these different interfacial structures can exist next to each other, just as different ORs between precipitate and matrix can exist simultaneously in a sample.

An estimate for the equilibrium stand-off distance of misfit dislocations can be obtained from a model given in Ref. [21] which indicates that a stand-off requires a large mismatch in elastic constants across the interface (which is often the case at metal/oxide interfaces), a high shear strength of the interface and a small mismatch between metal and oxide along the interface. For the Ag/Mn_3O_4 interface the calculated distance for an isolated interfacial dislocation is $0.24 \pm 0.1\ b_x$ (about 1/4 of the Burgers vector with direction parallel to the interface). For an array of interfacial dislocations instead of an isolated one the distance is somewhat larger. Still, the value would indicate that a stand-off is not expected in agreement with observations for a part of the interfaces. However, in the Nb/Al_2O_3 example given in Ref. [21] the calculated distance was also significantly smaller than the observed one (by about a factor of 3), which was explained by the neglect of the core-traction contributions to the image forces, which would have given an extra repelling force. Furthermore, a more direct, but qualitative indication that a stand-off may be expected is the low stacking fault energy of Ag [18], probably lower than the stacking fault energy at the interface. Since the disregistry parallel to the interface can be largely accounted for by Shockley partials and the tilt at the interface by Frank partials (as was seen above), these partials may then climb away from the interface into the material with low stacking fault energy. Also, the atomistic calculations indicated a small energy difference for the parallel

(a)

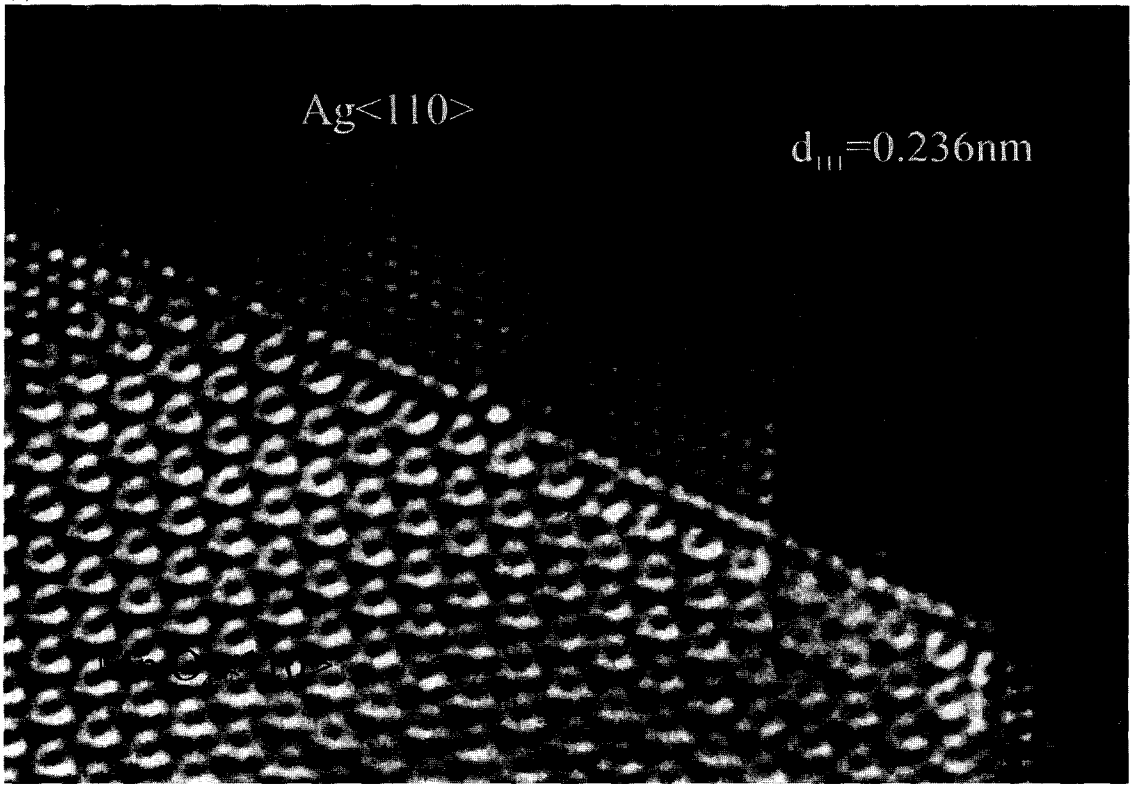

Fig. 12. *Caption on facing page.*

(b)

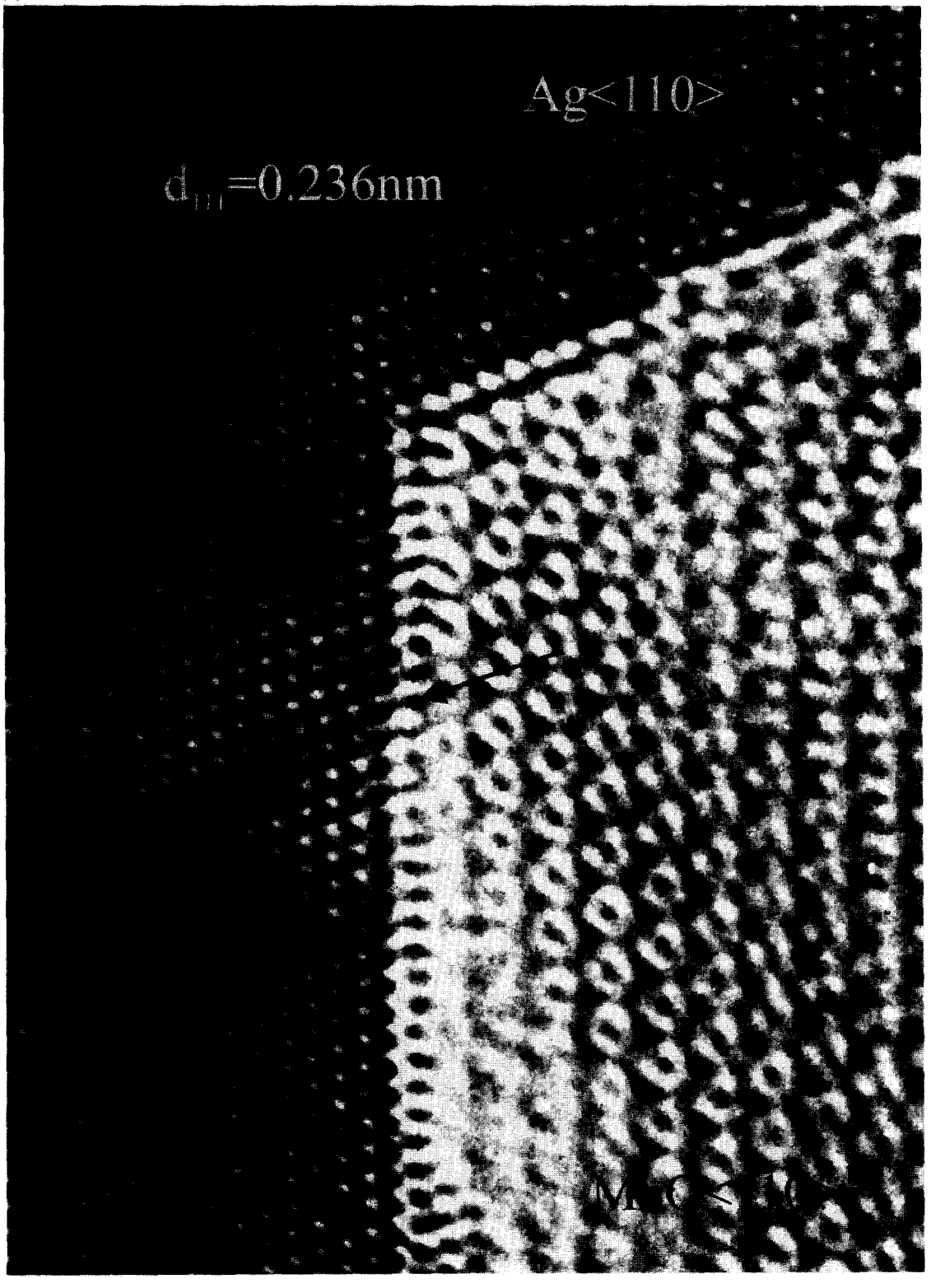

Fig. 12. (a) HRTEM image of a 3.5° tilted {111} Ag/Mn_3O_4 interface viewed along the common ⟨110⟩ of Mn_3O_4 and Ag; a "collapsed" ledge which improves the parallelism of the {111} planes of Ag and Mn_3O_4 at the interface can be observed. (b) HRTEM image of an approximately 1.1° tilted {111} Ag/Mn_3O_4 interface viewed along the common ⟨110⟩ of Mn_3O_4 and Ag; a ledge has collapsed which can be conceived as the dissociation of a Frank partial into a Shockley partial which was emitted along the {111} Ag making a large angle with the interface leaving a stacking fault behind and a stair-rod dislocation which remained behind at the interface: 1/3[111]→1/6[112] + 1/6[110].

interface with and without climb/dissociation of $1/3[11\bar{2}]$. The energy difference for misfit dislocations with and without stand-off is therefore probably relatively small, making both possible.

A part of the ledges exhibited relaxations in which they tend to collapse, improving the parallelism of $\{111\}$ of Ag and Mn_3O_4 at the interface; examples are shown in Fig. 12(a) and (b). The same phenomenon was observed and analysed earlier for tilted Ag/ZnO interfaces [22, 15]. Atomistic and continuum (linear anisotropic elasticity) calculations were performed to analyse these collapsing ledges in Ag/ZnO. The relaxation of a ledge can be conceived as a dissociation of a Frank partial (which was also observed above in Fig. 11 at the ledges in Ag/Mn_3O_4) into a Shockley partial which is emitted along the $\{111\}$ Ag making a large angle with the interface and a stair-rod partial which remains at the interface: $1/3[111] \rightarrow 1/6[112] + 1/6[110]$. Results of the atomistic calculations for the relaxations of the ledges in Ag/ZnO are shown in Fig. 13: 13(a) shows the starting configuration before relaxation with the full ledge-steps at the interface, 13(b) shows the resulting structure after relaxation and in 13(c) the structure of 13(b) is summarized by indicating the position and orientation of the close-packed Ag planes. In Fig. 13 it can be seen that at the interface the planes of metal and oxide have almost become parallel due to the relaxation. Comparing the positions of Ag atoms around the dissociated Frank partial as given by the atomistic calculations for Ag/ZnO [Fig. 13(b)] and as observed experimentally in Ag/Mn_3O_4 (Fig. 12), the similarity in the qualitative sense is remarkable, especially between Figs 13(b) and 12(a). Apparently the ledges in Ag accounting for the tilt with an oxide exhibit a similar mechanism for the relaxation independent of the exact nature of the oxide. The actual (equilibrium) separation between stair-rod and Shockley, however, will apart from the mismatch between Ag and oxide along the interface depend on the amount of tilt (i.e. the separation between the stair-rods at the interface) and on the relative elastic constants of Ag and the oxide. Such a dependency can be observed by comparing Figs 11, 12(a) and 12(b). The amount of tilt decreases significantly for the relevant interfaces shown in these three figures, i.e. about 7.6° (Fig. 11), 3.5° [Fig. 12(a)] and about 1.1° [Fig. 12(b)], whereas the separation between stair-rod and Shockley increases significantly in this order, i.e. no separation (no dissociation of the Frank partial at all), a separation of about 1.1 nm and a separation of 1.9 nm. The increase of (equilibrium) separation distance between stair-rod and Shockley with decreasing tilt is in qualitative agreement with the anisotropic elasticity calculations performed [22, 15].

The above mechanism in which a more parallel interface is achieved by emission of Shockley partials from a tilted interface, i.e. an interface for which the two planes at opposite sides of the interface want to be parallel but actually make a small angle with each other, is not restricted to metal/oxide interfaces. Also at grain boundaries in principle the same mechanism has recently been observed and analysed in detail [23]. The requirement for the observation of this mechanism is that phases with a low stacking fault energy are involved, and Ag fulfils this requirement well.

Finally, tetragonal twinning (i.e. on $\{011\}$) is observed in the Mn_3O_4 precipitates (with 1–4 twinning planes in typically 10-nm sized precipitates) producing shape changes that partly relax the misfit in shape between the tetragonal structure of the oxide and the cubic structure of the matrix. This tetragonal twinning observed in Mn_3O_4 precipitates in both Ag and Cu is the subject of a subsequent paper [24].

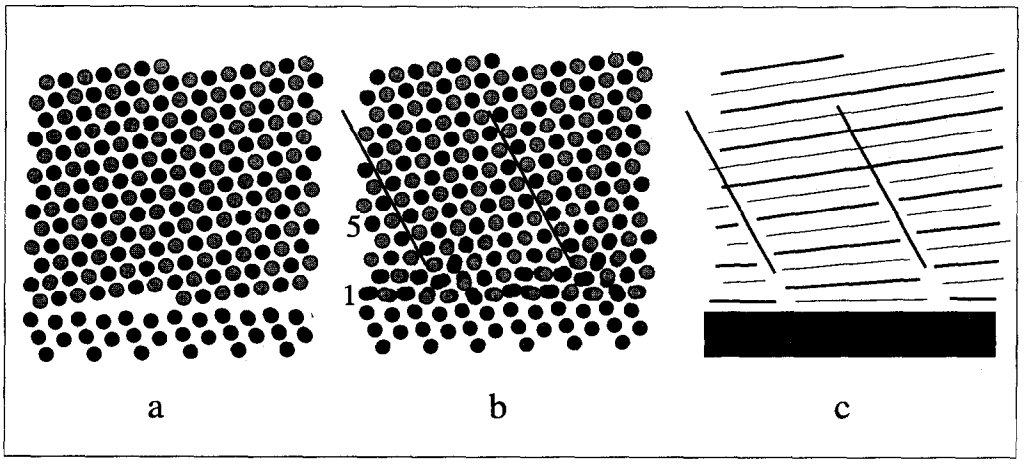

Fig. 13. Results of atomistic calculations for a tilted Ag/ZnO interface where the $\{111\}$ Ag is tilted 7.3° around $\langle 1\bar{1}0\rangle$ Ag with respect to the $\{0\bar{1}11\}$ ZnO. (a) Starting configuration for the atomistic calculations. (b) Configuration after relaxation to minimum energy ($\alpha = 2$). (c) Representation of the results shown in (b) giving the position and orientation of the close-packed Ag planes.

4. CONCLUSIONS

Internal oxidation of Ag–3 at.% Mn results in Mn_3O_4 precipitates with octahedron shape owing to {111} facets. Owing to the tetragonality of Mn_3O_4 not all eight {111} planes of metal and oxide can be parallel simultaneously. An equal tilt between {111} of metal and oxide on all eight interfaces of 3.8° can exist, but it appeared more favourable to align {111} planes for one pair of facets parallel in Ag and Mn_3O_4. At non-parallel {111} interfaces, tilted up to 7.7° around ⟨110⟩, ledges with direction ⟨110⟩ and height 1/4⟨112⟩ (the third index may not be permuted, because it is fixed by the *c*-axis of Mn_3O_4) are present in Ag. An essentially one-dimensional mismatch along ⟨112⟩ of 10.4% occurs between Ag and Mn_3O_4. This mismatch is generally accounted for by an array of dislocations with line direction ⟨110⟩ and alternating Burgers vector 1/6⟨112⟩ and 1/3⟨112⟩. At a part of the parallel and tilted interfaces dislocations were observed with a stand-off from the interface of one or two atomic spacings in the Ag and relaxations present at both these parallel and tilted {111} interfaces were clearly observed in HRTEM images. Guided by atomistic calculations the relaxations at the parallel {111} interfaces are ascribed to dissociation of the unfavourable 1/3⟨112⟩ Burgers vector into more favourable Shockley partials. At the tilted interfaces the ledges corresponding to the tilt between the {111} planes can collapse, improving the parallelism of {111} planes of metal and oxide at the interface. The mechanism behind this collapse is the dissociation of a Frank partial into a Shockley partial which is emitted into Ag along the {111} making a large angle with the interface and a stair-rod which remains at the interface.

Based on strain energy the Mn_3O_4 precipitates in Ag should have a plate shape with (001) as dominant facet. This is not observed. Apparently, the interfacial energy at the metal/oxide interface dominates over the strain energy and determines OR and precipitate shape.

Acknowledgements—The work described in this paper is part of the research program of the Foundation for Fundamental Research of Matter (FOM-Utrecht). The authors thank W. P. Vellinga for valuable discussion.

REFERENCES

1. Ernst, F., *Mater. Sci. Engng Rep.*, 1995, **R14,** 97.
2. Kooi, B. J., Groen, H. B. and De Hosson, J. Th. M., *Acta mater.*, accepted.
3. Kilaas, R., *Proc. 49th Annual EMSA Meeting*, 1991, p. 528.
4. Stadelmann, P., *Ultramicroscopy*, 1987, **21,** 131.
5. Vellinga, W. P., De Hosson, J. Th. M. and Vitek, V., *Acta Mater.*, 1977, **45,** 1525.
6. Wyckoff, R. W. G., *Crystal Structures*, 2nd edn. Interscience Publishers, New York, 1963.
7. Ernst, F., Pirouz, P. and Heuer, A. H., *Phil. Mag.*, 1991, **63,** 259.
8. Ernst, F., *Mater. Res. Soc. Symp. Proc.*, 1990, **183,** 49.
9. Lu, P. and Cosandey, F., *Ultramicroscopy*, 1992, **40,** 271.
10. Jang, H., Seidman, D. N. and Merkle, K. L., *Interface Sci.*, 1993, **1,** 61.
11. Chen, F. R., Chiou, S. K., Chang, L. and Hong, C. S., *Ultramicroscopy*, 1994, **54,** 179.
12. Vellinga, W. P. and De Hosson, J. Th. M., *Mater. Sci. Forum*, 1996, **207–209,** 361.
13. Chan, D. K., Seidman, D. N. and Merkle, K. L., *Phys. Rev. Lett.*, 1995, **75,** 1118.
14. Benedek, R., Minkoff, M. and Yang, L. H., *Phys. Rev. B. Lett.*, 1996, **54,** 7697.
15. De Hosson, J. Th. M., Vellinga, W. P., Zhou, X. B. and Vitek V., in *Stability of Materials*, ed. A. Gonis, P. E. A. Turchi and J. Kudronovsky. Plenum Press, New York, 1996, p. 581.
16. Finnis, M. W. and Sinclair, J. E., *Phil. Mag. A*, 1984, **50,** 45.
17. Ackland, G. J., Tichy, G., Vitek, V. and Finnis, M. W., *Phil. Mag. A*, 1987, **56,** 735.
18. Hirth, J. P. and Lothe, J., *Theory of Dislocations*. McGraw-Hill, New York, 1968.
19. Schoenberger, U., Andersen, O. K. and Methfessel, M., *Acta metall. mater.*, 1992, **40,** S1.
20. Smith, J. R., Hong, T. and Srolovitz, D. J., *Phys. Rev. Lett.*, 1994, **72,** 4021.
21. Mader, W. and Knauss, D., *Acta metall. mater.*, 1992, **40,** S207.
22. Vellinga, W. P. and De Hosson, J. Th. M., *Acta mater.*, 1977, **45,** 933.
23. Rittner, J. D., Seidman, D. N. and Merkle, K. L., *Phys. Rev. B*, 1996, **53,** 4241.
24. Kooi, B. J., Groen, H. B. and De Hosson, J. Th. M., *Proc. EUROMAT97*, Vol. 4. Neth. Soc. for Materials Science, Zwÿndrecht, The Netherlands, 1997, p. 17.